

The effect of sea level changes on fault reactivation potential in Portugal



M.C. Neves^{a,c,*}, J. Cabral^{b,c}, K. Luttrell^d, P. Figueiredo^{b,c}, T. Rockwell^e, D. Sandwell^f

^a Universidade do Algarve, Campus de Gambelas, 8005 139 Faro, Portugal

^b Departamento de Geologia, Faculdade de Ciências, Universidade de Lisboa, Campo Grande, 1749-016 Lisboa, Portugal

^c Instituto Dom Luiz, Universidade de Lisboa, 1749-016 Lisboa, Portugal

^d Louisiana State University, Baton Rouge, LA, USA

^e San Diego State University, San Diego, CA, USA

^f Scripps Institution of Oceanography, La Jolla, CA, USA

ARTICLE INFO

Article history:

Received 4 May 2015

Received in revised form 21 July 2015

Accepted 25 July 2015

Available online 10 August 2015

Keywords:

Sea level rise
Coulomb stress
Slip tendency
Flexure
Seismicity

ABSTRACT

The aim of this study is to assess the impact of sea level changes on both the stress field and the potential of fault reactivation in west Iberia. The analysis is applied to a set of five active faults distributed across Portugal, selected for representing predominant fault directions and for being seismically active. The results show that the rise of sea level since the Last Glacial Maximum has produced flexural effects with distinct impacts on different faults. The Coulomb stress changes induced by the sea level rise along the S. Marcos-Quarteira (south Portugal) and the Horseshoe (offshore SW Iberia) faults are found to be extremely small, independently of the elastic plate thickness. These faults are thus unaffected by flexural effects related to ocean loading, and are unlikely to possess any paleoseismic record of this phenomenon. In contrast, the eustatic sea level rise during the late Pleistocene could have raised the Coulomb stress by 0.5–1 MPa along the Manteigas–Vilariça–Bragança (north Portugal) and Lower Tagus Valley (Lisbon area) fault systems. Such stress perturbations are probably sufficient to impact the seismic cycle of the Manteigas–Vilariça–Bragança fault, bringing it closer to failure and possibly triggering the earthquake clusters that have been observed in previous paleoseismologic studies.

© 2015 Elsevier B.V. All rights reserved.

1. Introduction

The Portuguese territory (west Iberia) is currently undergoing tectonic deformation due to convergence between Iberia and Nubia, resulting in the reactivation of faults and the generation of infrequent large earthquakes such as the 1755 Lisbon earthquake. Geologic observations onshore indicate fault slip rates in the range of 0.005–0.5 mm/year, which are consistent with a low rate of tectonic activity and long recurrence intervals for maximum (M 6–7) earthquakes (e.g. Cabral, 2012). Paleoseismic studies have demonstrated that some faults have experienced recurrent late Quaternary activity, especially in NE Portugal where there is evidence of paleo-earthquake clustering during the Pleistocene (Rockwell et al., 2009). However, most large historical earthquake activity has been located in the central region of Portugal, within or near the Lower Tagus Valley (Lisbon area), while most of the present instrumental seismicity concentrates in the SW offshore region (Fig. 1a).

Based on current observations, there are fundamental questions as to how the long-term strain has been partitioned through time and space in Portugal. Most natural earthquakes result from tectonic

processes that act at geologic time scales (>1 Ma). Nonetheless, other processes acting at shorter time scales may induce Coulomb stress changes (as small as 0.1–1 MPa) capable of triggering earthquakes on faults that are already close to failure (King et al., 1994; Stein, 1999). One important class of such processes comprises the impacts of the climatic system on the tectonic system. An increasing body of evidence shows that seismicity rates can be affected by a wide range of meteorological and climate phenomena such as seasonal changes in precipitation (e.g. Bettinelli et al., 2008; Bollinger et al., 2007), snow loads (Heki, 2001), water loading and unloading effects at reservoirs (e.g. Simpson et al., 1988; Gahalaut et al., 2007) and lakes (e.g. Brothers et al., 2011; Kaufmann and Amelung, 2000), as well as isostatic rebound following glacier melting (e.g. Grollmund and Zoback, 2000; Hetzel and Hampel, 2005). Recent studies propose that fast erosion rates linked to high storminess are also a prominent mechanism for inter-seismic loading of active faults (Steer et al., 2014).

In this study, we focus on sea level changes associated with the Milankovitch cycle, which have been proposed to have a significant impact on the seismic cycle of near shore plate boundary fault systems (Luttrell and Sandwell, 2010) and on the occurrence of submarine landslides at passive continental margins (Brothers et al., 2013). These previous works have shown that the loading rates due to time varying surface water loads are generally one to several orders of magnitude lower than the tectonic loading rate. Their ability to affect the seismic

* Corresponding author at: Universidade do Algarve, FCT, ED8, Campus de Gambelas, 8005 139 Faro, Portugal. Tel.: +351 289800900 7361; fax: +351 2898000069.
E-mail address: mcneves@ualg.pt (M.C. Neves).

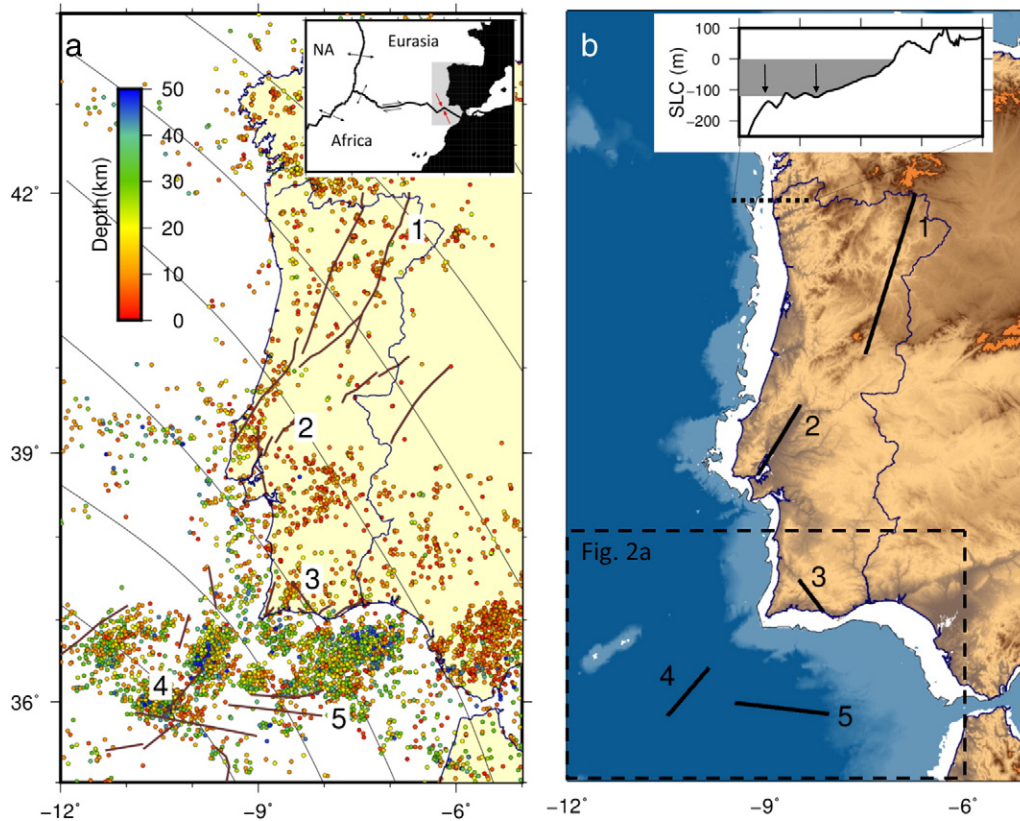


Fig. 1. (a) Map view of the study area with fault traces from the QAFI database (www.igme.es/infoigme/applications/qafi) and maximum horizontal compressive stress trajectories (solid lines) from de Vicente et al. (2008). Numbers indicate the faults analyzed in this study: (1) Vilarica, (2) Lower Tagus Valley, (3) Quarteira, (4) Horseshoe and (5) SWIM (north fault). Dots show the epicentres in the period between 1964 and 2014 taken from the ISC database (www.isc.ac.uk) with hypocentre depth in color scale. (b) White areas show the migration of the shoreline in western Iberia since the Last Glacial Maximum. A topographic profile across the continental margin at 42°N illustrates the extra vertical load (~120 m thick gray layer with black arrows) exerted as a result of sea level change (SLC) during that period. The black dashed rectangle depicts the offshore area presented in Fig. 2a.

cycle is therefore enhanced for regions of particularly low tectonic loading rate, such as west Iberia. As a possible evidence of the causal relationship between increased seismicity and ocean loading, Luttrell and Sandwell (2010) have suggested that the paleo-earthquake cluster found in NE Portugal could be due to rapid sea level rise during the late Pleistocene. Here, we will investigate if this hypothesis is indeed possible.

The Coulomb stress perturbations are calculated for a set of five active faults, geographically apart, that were selected for representing important fault directions and for being among the most seismically active in Portugal. The impact of the ocean loading perturbations, and therefore their probability of detection, depends on the background potential of fault reactivation. Since the fault reactivation potential due to tectonic loading has remained constant at the scale of the eustatic oscillations (10^4 – 10^5 years) the central question is to know how the stress changes induced by sea level rise compare with the “existing” reactivation potential at each fault.

In order to evaluate the reactivation potential in response to the tectonic loading we rely on a model of the current stress field in west Iberia (Neves et al., 2014) and perform a slip tendency analysis. The main aims of this study are therefore to: (1) estimate the reactivation potential of some of the most important faults in Portugal considering the present tectonic loading, and (2) model the lithospheric bending associated with ~120 m of eustatic sea level rise since the Last Glacial Maximum, and quantify the resulting Coulomb stress perturbations induced on the selected faults. Based on the modeling results we examine the possible relations between paleo-earthquakes and sea level changes and identify preferential targets for future paleo-seismological studies. This offers new insights into the long-term behavior of the faults in Portugal, within the framework of climate and tectonic interactions.

2. Tectonic setting

2.1. Active tectonics

The tectonic setting of mainland Portugal, characterized by a NW–SE trending maximum horizontal compressive stress (SH_{max} , Fig. 1a), generates significant neotectonic activity, of which the regional seismicity is a current expression (e.g. Borges et al., 2001; Ribeiro et al., 1996). The neotectonic deformations include two major interrelated components that may be distinguished and independently analyzed: vertical movements of the lithosphere, resulting from large scale folding and isostatic adjustments (e.g. Cloetingh et al., 2002) and active faulting. Active faults were largely conditioned by reactivation of pre-existent structures, namely Variscan faults in Paleozoic basement, and faults in Mesozoic extensional basins and in Alpine Cenozoic compressive and strike-slip basins. Fault activity shows a predominance of ~E–W to NE–SW reverse faults and ~N–S to NNE–SSW left-lateral strike-slip faults, reactivated under the present stress field (Cabral, 1995, 2012, and references therein). The present work focuses on some of these active faults, which are briefly described below.

2.1.1. The Vilarica fault

The Manteigas–Vilarica–Bragança fault (hereafter called Vilarica) is a prominent NNE–SSW trending strike-slip fault in West Iberia (Fig. 1, fault 1). Together with the Penacova–Régua–Verin fault, located 60 km to the west, it has been acting as a transfer zone of deformation between the Cantabrian Mountains and the Iberian Central System since the Eocene (de Vicente et al., 2008). With a length of approximately 220 km, the Vilarica fault has undergone polyphase activity since the end of the Variscan Orogeny, producing significant displacements of the

Variscan basement rocks, with a maximum left-lateral offset of 9 km in its central area (Cabral, 1989, 1995, 2012).

The scarcity of geological units that might serve as references for studying the post-Paleozoic behavior of the Vilarica fault makes it difficult to constrain its reactivation history. Nevertheless, the regional geomorphic expression and the occurrence of faulted Cenozoic sediments preserved in some depressed areas along the fault-zone, indicate that this structure was reactivated in Tertiary and Quaternary times. Present fault activity is also evidenced by some low magnitude instrumental seismicity and two moderate (estimated M5+) historical earthquakes in 1751 and 1858 (Vilanova and Fonseca, 2007).

Evidence of predominant left-lateral strike-slip during Plio-Quaternary time is mainly provided by (1) fault outcrop kinematic indicators, (2) presence of several strike-slip tectonic basins along the fault zone (such as the Longroiva and Vilarica basins), (3) the presence of some compressive structures interpreted as push-ups developed at restraining bends (such as Bornes Mountain) and (4) late Quaternary stream deflections and (5) paleoseismic work that has shown repeated late Quaternary left-lateral displacements (Rockwell et al., 2009). At the southern end of the Vilarica basin, where the Douro river is apparently left-laterally offset 1 km by the Vilarica fault, an average slip rate of 0.4 mm/year has been inferred for the last 2.5 Ma (Cabral, 1995, 2012). In the same region, a probable left lateral offset of circa 40–50 m of a nearby creek indicates an average strike slip displacement rate of 0.2 to 0.5 mm/year, in the late Quaternary (Rockwell et al., 2009).

2.1.2. Lower Tagus Valley fault

The Lower Tagus Valley (LTV) fault system consists of several stepped fault segments trending parallel to the NNE–SSW longitudinal direction of the Lower Tagus Cenozoic Basin (Fig. 1a). The Cenozoic basin comprises up to about 2000 m of Tertiary sediments, and also contains a thick (up to 70 m) Upper Pleistocene to Holocene alluvial cover due to Last Glacial Maximum drainage incision followed by aggradation. The NNE–SSW fault segments show evidence of Neogene vertical displacements, with mostly high angle reverse or oblique left-lateral reverse senses of displacement. These segments are linked by secondary WNW–ESE to NW–SE faults that also accommodate significant vertical motion and delimit structural lows and highs (Cabral, 1995, Cabral et al., 2003; Carvalho et al., 2006). Although this fault system has been identified in the basement, a single fault trace is not clearly defined at the surface (Carvalho et al., 2014). For modeling purposes, the LTV fault is considered to correspond to the locations of the Azambuja and Vila Franca de Xira faults, assuming that they are linked at depth (Fig. 1b, fault 2).

The LTV region, which includes the densely populated area of Lisbon, has been affected by historical, local, M 6–7 intraplate earthquakes that have caused severe damage and many casualties, as in 1344, 1531 and 1909 (Stich et al., 2005; Teves-Costa et al., 1999). Since the 1909 event, the instrumental seismicity in the LTV has been low and diffuse. Although this region has been the subject of several neotectonic studies, major uncertainties on the seismogenic structures persist due to the low estimated slip rates (0.05–0.1 mm/year), the presence of the thick sedimentary cover that conceals the faults, and the likely interference of rupture directivity and site effects (Cabral et al., 2013; Carvalho et al., 2014).

2.1.3. S. Marcos–Quarteira fault

The S. Marcos–Quarteira fault zone (hereafter referred to as the Quarteira fault), is a NW–SE trending structure that extends for approximately 40 km in the south of Portugal (Fig. 1, fault 3). It is a major regional tectonic structure inherited from the Variscan Orogeny, which controlled the evolution of the Algarve basin during the Mesozoic, separating it into two blocks that evolved differently. It was reactivated during the Cenozoic and, since the Neogene, it has controlled the evolution of the regional landscape, namely of the Serra de Monchique and Serra do Caldeirão mountains, located west and east of the fault,

respectively. The extension of this fault to the offshore, together with other related structures, has been recognized, but its degree of activity and relationship with the onshore section is still not clearly understood (Carvalho et al., 2012; Terrinha et al., 2009).

The neotectonic activity of the Quarteira fault is better demonstrated in the SE sector by the presence of intensely deformed Pleistocene clastic sediments. In addition to being tilted and faulted, these detrital deposits are strongly folded by fault drag and show convolute bedding, suggesting liquefaction and fluidization that probably occurred during large magnitude earthquakes (Dias, 2001). Although there are no known major historical earthquakes that are clearly associated with this fault zone, there are historical moderate magnitude earthquakes with strong intensities that may have occurred along this structural trend. Although no surface rupture is known or was recognized, the Quarteira fault shows some control on the regional seismicity pattern, expressing some alignments of epicenters and apparently working as the NE boundary of an area of higher seismicity at the SW.

2.1.4. The Horseshoe fault

The region offshore SW Iberia accommodates the convergence between the Nubia and Iberia plates by diffuse brittle deformation, as evidenced by widely developed tectonic structures with different orientations and kinematics (Fig. 2a). In recent years numerous campaigns including deep-sea drilling and submersible expeditions, and geophysical surveys with seismic, bathymetric and potential field data acquisition have been conducted in this area. Most of these surveys aimed at mapping and characterizing the tectonic structures associated with the Nubia–Eurasia plate boundary, at locating the source of the 1755 Lisbon Earthquake or at determining the nature of the crust across the different tectonic domains present in the Gulf of Cadiz (e.g. Terrinha et al., 2003; Rosas et al., 2012; Martínez-Lorientte et al., 2014; and references therein). As a result of this research, several important seafloor folds and fault scarps were identified, among which is the Horseshoe Thrust Fault (HTF) (hereafter called Horseshoe) (Fig. 1, fault 4; Fig. 2a). It is considered one of the most significant structures in the Gulf of Cadiz, displaying a scarp ~1000 m high in its northeasternmost segment and showing evidence of activity since at least ~10 Ma (e.g. Gràcia et al., 2003; Terrinha et al., 2009). This major thrust was previously proposed to share a common detachment with other NE–SW thrusts in the area, namely with the Marquês de Pombal Thrust Fault (MPTF), with which it was thought to represent a possible source for the 1755 Lisbon Earthquake (Gràcia et al., 2003; Terrinha et al., 2009) (Fig. 2a). As a whole these NE–SW thrusts have been interpreted as early manifestations of the tectonic reactivation of the southwest Iberian margin, representing the initiation of subduction along this segment of the Atlantic passive margin (Duarte et al., 2013; Ribeiro et al., 1996).

At the present day an important part of the instrumental seismicity in the Gulf of Cadiz occurs beneath the Horseshoe Abyssal Plain (Fig. 1a). Most events have low to moderate magnitudes showing reverse and strike-slip fault plane solutions that are compatible with NW–SE to NNW–SSE shortening (Fig. 2a). A direct correlation between earthquake location and known major tectonic structures is not straightforward, because most earthquakes occur in the lithospheric mantle (30–60 km depth) whilst in the seismic profiles the major faults are imaged at maximum depths of only ~6–10 km (Geissler et al., 2010; Rosas et al., 2012).

2.1.5. The SWIM fault

The SWIM (Southwest Iberian Margin) fault (Fig. 1, fault 5; Fig. 2a) is part of a fault system corresponding to a broad band of deformation, extending across the entire Gulf of Cadiz domain (along 600 km), and essentially characterized by sets of major deep rooted, sub-vertical, dextral strike-slip faults (Bartolome et al., 2012; Zitellini et al., 2009). The SWIM faults, which are thought to be active since at least ~1.8 Ma (Rosas et al., 2009), were interpreted as the precursor of a new (dextral) transcurrent plate boundary in the Gulf of Cadiz (Zitellini et al., 2009).

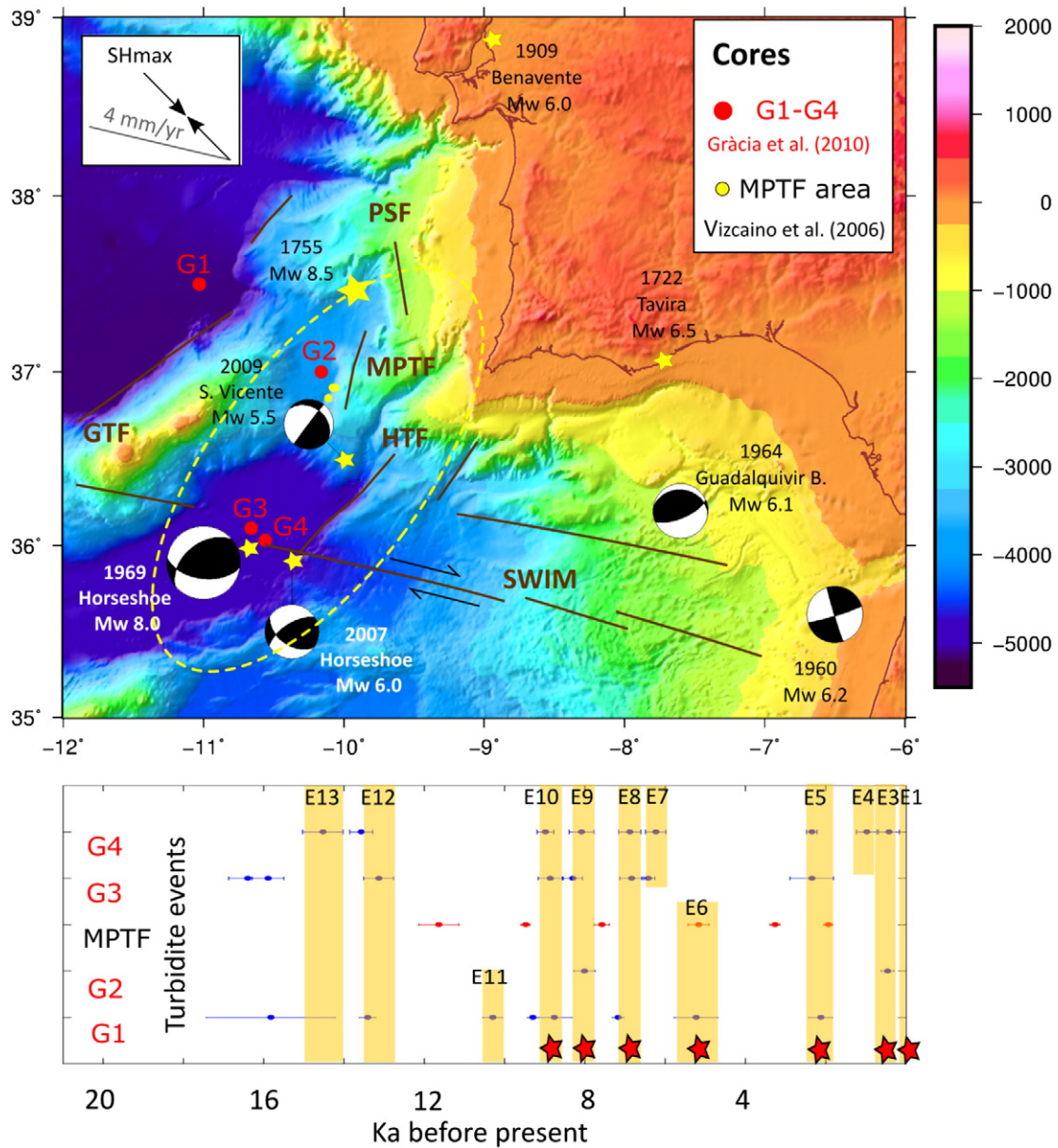


Fig. 2. (a) Simplified tectonic setting of the SW Iberian margin showing the location of sediment cores (G1–G4) and gravity cores in the Marqués de Pombal Thrust Fault (MPTF) area (modified from Gràcia et al., 2010). Shaded relief from a blend of high resolution data (w3.ualg.pt/~jluis/mirone/data_links). Yellow stars depict the location of large historical and instrumental earthquakes (possible location of the 1755 Lisbon earthquake inside the yellow dashed ellipse). Focal mechanisms are from Pro et al. (2013). Inset (showing the average direction of the 4 mm/year convergence rate between Nubia and Iberia and the average direction of the maximum horizontal stress-SHmax) and active faults (brown lines) are from Rosas et al. (2012). GTF: Gorringe Thrust Fault; HTF: Horseshoe Thrust Fault; PSF: Pereira de Sousa Fault. SWIM lineaments are based on the tectonic interpretation of Zitellini et al. (2009)). (b) Chronology of turbidite events (E3–E13) presented by Gràcia et al. (2010) based on piston cores (G1–G4) and gravity cores from a local study in the MPTF area (Vizzaino et al., 2006). Red stars depict widespread turbidite events detected in cores from at least two of the different depositional areas.

According to thin-sheet numerical models in the Gulf of Cadiz the SWIM faults are not likely to be slipping at more than 1–2 mm/year (Cunha et al., 2012).

A local network of OBS deployed in the Horseshoe Abyssal Plain in 2007 recorded numerous low to moderate magnitude earthquakes ($M_L = 2.2\text{--}4.8$) in connection with the SWIM faults (Geissler et al., 2010). Most of these events concentrated at the intersection between the SWIM and Horseshoe faults at depths of 40–60 km. The intense seismic activity and the significant heterogeneity in the focal mechanism solutions have been attributed to the tectonic interference between strike-slip and thrust faulting (Rosas et al., 2012). Moreover, the depth discrepancy, between the observed (upper crust) interference fault-pattern and the (lithospheric mantle) seismicity, has been interpreted as a manifestation of similar thrust–wrench tectonic interference at different lithospheric depths.

2.2. Paleoseismologic evidence

2.2.1. Offshore SW Iberia

Although characterized by low to moderate seismic activity, the SW Iberian margin has been the source of large ($M_w > 6$) and destructive earthquakes, such as the 1722, 1755 and 1969 events (Fig. 2a), some of them (e.g. 1722, 1755) accompanied by devastating tsunamis (Baptista et al., 2003, 2007). The most updated geological and geophysical investigations in the area have recently been used to define large earthquake (and tsunami) generation models in the Gulf of Cadiz (Matias et al., 2013). According to that study, the recurrence periods for a magnitude 8 event, for example, vary between 3600 and 7200 years, on a single fault. The occurrence of a “1755-like” earthquake implies the coseismic rupture of several faults and, for an average slip rate of 1 mm/year, the estimated recurrence period of such an extreme event

is c. 10 ka. Such long seismic cycles make the seismic hazard assessment particularly difficult.

An alternative source of paleoseismic evidence in continental margins is the use of landslide and turbidite records as proxies of paleoseismic activity. Gràcia et al. (2010) proposed that, in the Gulf of Cadiz, earthquakes are the most likely triggering mechanism for synchronous widely-spaced distributed turbidites during the Holocene. A thorough analysis of strategically located sediment cores (Fig. 2a), allowed to establish the chronology of the turbidite deposits and to conduct a synchronicity test integrating data from previous studies (García-Orellana et al., 2006; Vizcaino et al., 2006). The results revealed a record of episodic deposition of turbidites, with a total of seven widespread (E1, E3, E5, E6, E8, E9 and E10) events during the Holocene (Fig. 2b). Some of the most recent events correlate with the most important historical earthquakes in the area (e.g. events E1 and E3 correlate with the 1969 and 1755 earthquakes, respectively). Based on the turbidite frequency, Gràcia et al. (2010) proposed a recurrence interval for great earthquakes of approximately 1.8–2.0 ka. The only event that was directly associated with sea level rise was E9, which occurred immediately after the 8.2 ka climatic event (meltwater pulse MPW-1A in Fig. 3a). However, previous events (E10, E11, E12 and E13) may also be associated with sea level changes via the impact of ocean loading on increased seismicity rates.

2.2.2. Onshore Portugal

Various efforts have been conducted in the past few years to determine the paleoseismic history of several faults of Portugal mainland, but unequivocal evidences for late Pleistocene activity is rare.

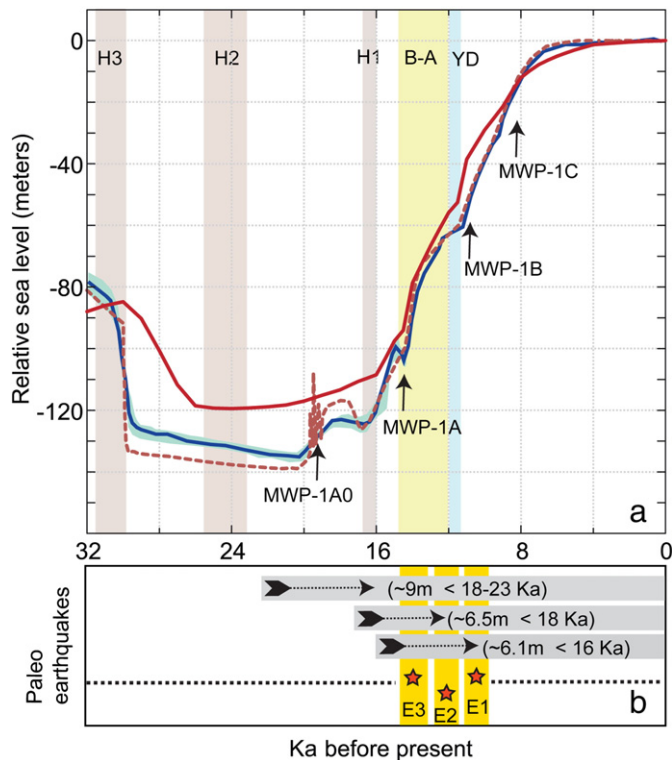


Fig. 3. (a) Relative sea level curves according to distinct authors: red curve represents the prediction of the ICE-5G (VM2) model for the Barbados site (Peltier and Fairbanks, 2006); blue curve represents an estimate that includes isostatic corrections with a high-viscosity mantle and its 95% probability limiting values; dotted pink line is a similar estimate assuming a low viscosity mantle (Lambeck et al., 2014). Significant melting water pulses (MWP) climatic events are overlapped: (H3) Heinrich event 3, (H2) Heinrich event 2, (H1) Heinrich event 1, (B-A) Bølling-Allerød interstadial, (YD) Younger Dryas stadial. (b) Cluster of large magnitude events (E1, E2 and E3) that occurred at the Vilarica fault in the period between 14.5 and 11 ka (Rockwell et al., 2009). Amount of displacement and age of deformation is indicated.

Paleoseismological studies along the Vilarica fault were conducted by Rockwell et al. (2009) at two sites near the southern end of the Vilarica basin. The occurrence of at least two and probably three events in the past 14.5 ka was determined at one site, suggesting an average return period of about 5–7 ka, although the events appear to have occurred as a cluster in the interval between 14.5 and 11 ka, or shortly thereafter, suggesting a return period of less than 2 ka between events within the cluster. At another site, several trenches exposed the fault displacing alluvial channel deposits dated to between 18 and 23 ka. A channel riser was traced into and across the fault to resolve c. 6.5 m of displacement after 18 ka and c. 9 m of slip after c. 23 ka, yielding a slip rate of 0.3–0.5 mm/year, which is consistent with the earlier, long term estimates. The period corresponding to the Vilarica earthquake cluster corresponds to the period when sea level rose about 50 m following the meltwater pulse 1A (MPW-1A) (Stanford et al., 2006), after the Last Glacial Maximum (Fig. 3).

The paleoseismological information argues for earthquakes in the M7+ range, with coseismic displacements of 2–3 m. A segmentation model of the Vilarica fault, comprising three segments of roughly 70 km each, may be obtained from the cartographic fault trace geometry and the geomorphic expression. A maximum M ~7 earthquake is thus expected, assuming rupture of one entire segment for that event, which is consistent with the paleoseismological data. Efforts to complete the paleoseismic record for the Vilarica fault, were conducted by Perea et al. (2010), but no other paleo-earthquakes, earlier or posterior to the events described by Rockwell et al. (2009), were recognized. These observations reinforce the idea that large magnitude earthquakes, that are likely to rupture the entire Vilarica fault length, do not occur periodically, but rather as a cluster of events.

3. Methods

3.1. Slip tendency analysis

In terms of the effective stress, which incorporates the effect of the pore fluid pressure, the critical condition for sliding on a pre-existing plane of weakness can be written as,

$$\mu = \tau/\sigma \quad (1)$$

where τ and σ are respectively the shear stress and the normal effective stress acting on the fault surface, and μ is the coefficient of friction. The slip tendency of a surface is defined as the ratio of the shear stress to the normal stress on that surface (Morris et al., 1996),

$$T'_s = \tau/\sigma \quad (2)$$

The fault planes that will more likely slip are those with a high ratio of shear to normal effective stress, close in value to μ . The slip tendency analysis is based on the fact that the slope of the failure criterion, i.e. the coefficient of friction, may span a range of values limited by Byerlee's experiments. Generally μ is in the range 0.6–1.0 (Byerlee, 1978). In a region dominated by a particular rock type the assumption of a specific μ determines the optimum angle θ for sliding, $2\theta = \tan^{-1}(1/\mu)$. This is the most favorable orientation of the fracture plane relative to the direction of maximum compression (Jaeger, 1969). In this plane the slip tendency is maximum, i.e. $T'_s = T'_s^{\max}$. A normalized slip tendency varying between 0 and 1 is defined by dividing the slip tendency by its maximum possible value, $T_s = T'_s/T'_s^{\max}$. The normalized slip tendency (simply designated as slip tendency hereafter) then ranges from 100% near the ideal fault orientation to 0% in planes perpendicular to the principal stress directions. To compute the slip tendency analysis we use the software developed by Neves et al. (2009) which is based on the formulation described in Appendix A. The method has been implemented in the form of a plug-in for the COULOMB software (Lin and Stein, 2004; Toda et al., 2005) and provides a graphical representation of the fault re-activation potential.

3.2. Plate bending from ocean loading

The effect of sea level changes on fault reactivation is modeled by treating the lithosphere as a thick elastic plate overlying a Maxwell viscoelastic half-space representing the asthenosphere. The strains due to ocean loading are considered small enough for infinitesimal strain theory to be valid, and therefore the total stress can be regarded as the sum of individual stress components (superposition principle). As we are not interested in the absolute state of stress, but rather on stress perturbations at the timescale of eustatic oscillations (10^4 – 10^5 years), we calculate the effect of sea level changes separately from other sources of stress that act at other time scales. For example, stresses associated with earthquake cycles (timescale 10^2 – 10^4 years) are not taken into account, and stresses due to tectonic loading (timescale > 1 Ma) are assumed to remain approximately constant at the timescale of sea level effects. The plate deflection and the 3D stress tensor are calculated using the method originally developed by Smith and Sandwell (2004) to model the earthquake cycle along the San Andreas Fault system, and latter adapted to compute the ocean loading effects on near shore fault systems (Luttrell and Sandwell, 2010). The 3D problem is solved analytically in the vertical and time dimensions (z, t), while the solution in the two horizontal dimensions (x, y) is developed in the Fourier domain to take advantage of the efficiency offered by the convolution theorem. The numerical implementation of the method involves generating a grid of vertical vector forces representing the spatially varying water load, taking the 2D horizontal Fourier transform of the grid, multiplying by the appropriate transfer functions and time-dependent relaxation coefficients, and finally applying an inverse Fourier transform function to obtain the stress and displacement components in the space domain.

The method has been thoroughly benchmarked against known analytical solutions, such as the elastic half-space solution at instantaneous time and the thin plate flexure solution at infinite time (Luttrell and Sandwell, 2010; Luttrell et al., 2007; Smith and Sandwell, 2004). Its main advantage over other alternative analytical and numerical methods (e.g. Crouch and Starfield, 1983; Okada, 1992) is that it includes a viscoelastic response to model the loading history and has the accuracy and speed necessary for computing both geometrically and temporally complex models of faulting. The duration of the viscoelastic response of the half-space is characterized by a single Maxwell relaxation time ($\tau_M = \eta/\mu_M$ where η and μ_M are the viscosity and the Maxwell rigidity, respectively) regardless of the wavelength of the load. The value assigned to the half-space viscosity determines the relaxation time of the asthenosphere and hence how quickly the elastic plate bends in response to the water load. For reasonable values of the asthenosphere viscosity (10^{19} – 10^{20} Pa s) the timescale of the half-space Maxwell relaxation time (10^2 years) is much shorter than the timescale of the sea level rise (10^4 years). As a consequence, we only observed the fully relaxed response of the model, which is equivalent to the flexural response of an elastic plate over a fluid half-space.

Once the flexural problem is solved, the 3D stress tensor induced by ocean loading can be used to estimate the seismic potential of suitably located faults. The seismic potential of a given fault is estimated by calculating the Coulomb differential stress (King et al., 1994) given by,

$$\Delta\sigma_c = \Delta\tau + \mu\Delta\sigma_n \quad (3)$$

where $\Delta\sigma_n$ and $\Delta\tau$ are the normal and shear stress changes on a fault plane and μ is the coefficient of friction. The normal and shear stress changes acting on a given plane are then computed using Eqs. (1) and (2) of the appendix. Right-lateral shear stress and tension are assumed to be positive. Whether a stress perturbation brings a fault closer to or further from failure is inferred by a change in the Coulomb differential stress. Failure is favored by positive Coulomb stress changes, which

can occur either from reduced normal stress (normal stress is negative in compression, so $\Delta\sigma_n > 0$ favors sliding) or increased shear stress.

4. Reactivation potential due to tectonic loading

4.1. Inputs and assumptions

In order to evaluate the potential of reactivation of a given fault we need to know: (1) the principal stress directions and the stress difference ratio R in the fault's region; (2) the geometry of the fault and (3) the coefficient of friction. Ideally, the slip tendency analysis should be based on indicators of the stress field at the scale of each fault, but in our study area this is not possible because stress indicators at that scale are either not available or do not have the required spatial resolution. As an alternative we use a simulation of the regional stress field at the scale of Iberia that has been obtained in a previous study (Neves et al., 2014). In that study the stress field was computed as the sum of a contribution from the plate boundary forces and a contribution from the gravitational potential energy (GPE) arising from topographic variation and lateral density heterogeneities. We used the geoid height as a measure of GPE and scored the models against both present-day strain rate and stress field data compilations. In this model (Fig. 4a) the GPE works against the plate boundary forces by reducing the SHmax magnitude, and causes the stress regime to gradually change from a thrust-faulting regime in the Gulf of Cadiz to a strike-slip regime in northern Portugal. As the stress field is 2D, we implicitly assume that one of the principal stresses is vertical. The GPE analysis relies on a long wavelength, thin plate approximation, so at the scale of each fault we assume laterally homogeneous conditions and use a constant (average) stress tensor. The principal stress magnitudes are not required since only the value of the stress difference ratio R is relevant to the slip tendency analysis. Regional inversions of moment tensor focal mechanisms in Iberia indicate R values of 0.5–0.75 in western Iberia and 0.1–0.5 in the Gulf of Cadiz (de Vicente et al., 2008; Stich et al., 2006). For every fault we compute the minimum and maximum slip tendency values corresponding to the two end-members of the regional R estimates.

Regarding the properties of the faults additional assumptions are required in order to make the analysis possible. Real faults exhibit deviations from planarity at all scales and are characterized by many heterogeneities that can locally trigger or arrest rupture propagation. Given the scale of our study and the overall uncertainties on fault properties we adopt a simple model of continuous planar faults with uniform properties based on the QAFI database (Table 1) (www.igme.es/infoigme/applications/qafi). Finally, there are no direct or indirect measures of the coefficient of friction, which may vary from fault to fault and even along one particular fault. For the sake of simplicity we adopt $\mu = 0.6$ for every modeled fault.

4.2. Results

It is important to point out that the slip tendency is not a predictor of fault slip, but an assessment of the likelihood of fault reactivation compared to a given stress threshold (or coefficient of friction). Fig. 4b shows the normalized slip tendency (T_s) computed using the average principal stress directions at each fault location. Higher (closer to 1) T_s values imply that a given fault is favorably oriented to the confining stress field, and therefore indicate a higher probability of slip. Previous studies in the Gulf of Cadiz have shown that even small changes in the orientation of the input stress tensor have a strong impact on the slip tendency distribution (Neves et al., 2009). To address the sensitivity of our results to the orientation of the input stress field, we have modeled the fault slip tendency considering deviations of $\pm 15^\circ$ in the input principal stress directions at each fault location. This range ($\pm 15^\circ$) is the same as the maximum azimuth misfit obtained when comparing the simulated stress field and the stress indicator data in our area of study (Neves et al., 2014). For each fault the values of T_s corresponding to

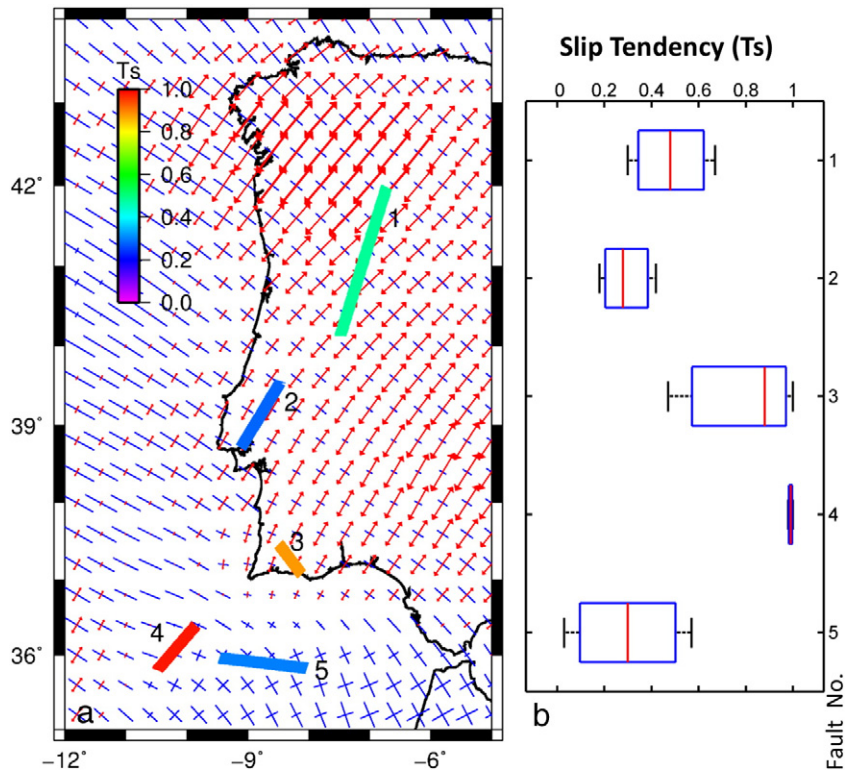


Fig. 4. (a) Average fault slip tendency (T_s) computed at each fault superimposed on the present day stress field used as input. A strike-slip stress regime is indicated by equal length tensional (red) and compressional (blue) pair of arrows. (b) Boxplot of the slip tendency computed at each fault considering both the R value range and an interval of deviations of $\pm 15^\circ$ from the average input stress directions. The central red bar is the median value, the edges are the 25th and 75th percentiles, and the whiskers extend to the most extreme estimates. Numbers indicate (1) Vilarica, (2) Lower Tagus Valley, (3) Quarteira, (4) Horseshoe and (5) SWIM faults.

the end-member values of both R and principal stress directions were combined into a single dataset (Fig. 4b). At each fault we obtain similar T_s estimates irrespective of the R values, so the observed spread is essentially due to the orientation of the stress tensor.

There is a first group of faults with median T_s values less than 0.5 that is classified as having low slip tendency due to tectonic loading. This group includes the Vilarica (No. 1), the Lower Tagus Valley (No. 2) and the SWIM (No. 5) faults. These faults are not locked (in fact all of them have median $T_s > 0.3$) but are also not susceptible to reactivation unless the slip threshold (coefficient of friction) is lower than 0.6. In some instances, the coefficient of friction in active faults may be much lower than 0.6, as documented in some field and laboratory studies (e.g. Colletini, 2011) or inferred from focal mechanism analysis (e.g. Middleton and Copley, 2014). Nonetheless, the relatively low slip tendencies that are predicted for these three faults are consistent with the neotectonic observations, namely the low estimated fault slip rates and the sparse and low magnitude instrumental earthquakes. Onshore, the estimated maximum fault slip rates are 0.5 mm/year and 0.1 mm/year for the Vilarica and Lower Tagus Valley faults, respectively (Sections 2.1.1 and 2.1.2). Offshore, the SWIM faults are not likely to slip

at more than 2 mm/year (Section 2.1.6) and show no significant seismic activity, except where they interact with the Horseshoe fault.

The second group of faults displays intermediate to high fault slip tendency and includes the Quarteira (No. 3) and Horseshoe (No. 4) faults. Compared to the other onshore faults analyzed in this study the Quarteira fault is the one with the highest probability of reactivation ($0.5 < T_s < 0.9$) under present tectonic loading. A large reactivation potential is supported by previous studies recognising the Quarteira fault as a major potential source of damaging earthquakes ($M > 5.5$) in the Algarve region (Dias, 2001). On the offshore, the Horseshoe fault stands out as the one showing the largest (maximum $T_s \sim 1$) slip tendency in the model. This result can be extrapolated to any of the similar NE–SW striking, westward verging thrust faults (e.g. Gorringer and Marquês de Pombal) that accommodate the on-going shortening in the Gulf of Cadiz. In fact these structures have been recognized as the most tectonically active structures in the region, and are probably capable of causing devastating earthquakes and tsunamis (e.g. Matias et al., 2013; Terrinha et al., 2003).

5. Stress changes from rising sea level

5.1. Inputs and assumptions

We model the stress at seismogenic depth due to rises in sea level using a thick elastic plate over a viscoelastic half space. One of the key model parameters is the elastic thickness T_e , which controls the flexural wavelength. In the continental lithosphere it is not uncommon to observe several co-existing flexural wavelengths in the same region. These observations often reflect lateral variations of integrated vertical strength or the existence of decoupling conditions between mechanically competent layers. For example, partial coupling/decoupling between the crust and mantle explains the superposition of different wavelengths (350–420 km and 180–200 km) of large-scale folding in Iberia (Cloetingh et al., 2002). The problem is frequently simplified by

Table 1
Fault geometric and kinematic parameters.

No.	Fault	Type	Average strike	Average dip	Average rake
1	Vilarica	Strike-slip left-lateral	020	90	0
2	Lower Tagus Valley	Oblique, left lateral	030	70	45
3	Quarteira	Strike-slip right lateral	146	90	180
4	Horseshoe	Reverse	45	30	90
5	SWIM	Strike-slip right lateral	105	90	180

focusing on the dominant wavelength of deformation and assuming a laterally homogeneous and uniformly thick elastic layer. We adopt this approach, which although simplified has proved to be remarkably robust and appropriate for a first-order assessment of the bending stresses. The mechanical and rheological structure of the west Iberia margin has been widely modeled for its implications on the long-term strength of stretched continental lithosphere and on the rupture mechanism of large earthquakes, such as the 1755 Lisbon earthquake (e.g. Pinheiro et al., 1992; Sallarès et al., 2013). In the southwest Portuguese margin the majority of these studies suggest mechanical coupling between the crust and mantle and the existence of a strong brittle plate, up to 50 km thick. To the south of Lisbon, combined 2D backstripping and gravity modeling techniques indicate that T_e increased with age since rifting, achieving values of ~35–50 km during the Miocene to recent period of compression (Cunha et al., 2010). These values compare well with regional estimates in the Iberian Peninsula of ~25–50 km obtained using the free-air admittance method (Pérez-Gussinyé and Watts, 2005) and from strength envelopes (Tesauro et al., 2012), but are substantially larger than the 17 ± 4 km range obtained using the Bouguer coherence method (Gómez-Ortiz et al., 2005). Given the wide range of existing estimates we consider T_e values between 25 and 55 km. Other important model parameters are the Young's modulus (E), Poisson's ratio (ν) and half-space viscosity (η). For both the plate and the half-space we assume $E = 70$ GPa and $\nu = 0.25$. The viscosity of the underlying half-space is assumed to be 10^{20} Pa s, corresponding to a Maxwell relaxation time of about 200 years. Since the sea level loading occurs over thousands of years, which is much greater than this relaxation time, the half-space behaves as an inviscid fluid and the stress models are insensitive to the assumed viscosity. In the assessment of the Coulomb stress changes the coefficient of friction is set to 0.6, as in the slip tendency analysis.

The vertical load results from a sea level rise of ~120 m over the past 20,000 years (Fig. 3a). The spatial variations in the vertical load are determined by the bathymetry and geometry of the continental margin (Fig. 1b, inset). To compute the exact shape of the vertical load, both in the offshore and near shore regions, we used the SRTM30_PLUS global bathymetric grid (Becker et al., 2009) with a lateral resolution of 30 s (~1 km). However, the eustatic sea level rise was not monotonic. Coral-based reconstructions suggest that about half (~50–60 m) of the global sea level rise since the Last Glacial Maximum occurred during the early Holocene (Fairbanks, 1989). The period between about 15 ka and 10 ka, in particular, was marked by the continued meltdown of ice sheets which led to a dramatic rise in sea level (Fig. 3). We also separately model this 5000 year period of loading and thereby address the effect of a relatively faster rate of sea level rise on the Vilariça fault in particular.

5.2. Results

Previous studies have shown that the extent to which faults in coastal areas can be affected by sea level changes depend not only on the thickness of the flexing plate but also on the shape of the coastline (Luttrell and Sandwell, 2010). The extent of the stress perturbation around western Iberia is shown in Fig. 5 for two specific values of the elastic plate thickness ($T_e = 25$ km and $T_e = 45$ km). In both cases the figure depicts the maximum shear stress $(\sigma_1 - \sigma_3)/2$ corresponding to the fully relaxed response of the elastic lithosphere to 120 m of sea level rise. It is clear that the larger the plate thickness, the larger the flexural wavelength (~150 (300) km for $T_e = 25$ (45) km) and, consequently, the more widespread the stress perturbations. The areas of greatest stress perturbations are predicted to occur offshore, particularly near Cape Finisterre (NW), Cape St. Vicente (SW) and in the vicinity of the Gibraltar Strait. These concentrations, which become more pronounced for larger values of T_e , are due to corner effects created by the geometry of the shoreline. The perturbation of a given fault is determined by the fault's location, in particular its distance to the coast, versus the plate

thickness, and its depth, in particular whether it lies above or below the flexural nodal plane. In Portugal, we verify that inland or offshore faults that are more than 100 km away from the coast, such as the Vilariça or the SWIM faults, do not experience stress changes caused by ocean loading unless the elastic plate is considerably thick ($T_e = 45$ km).

Whether the bending stresses promote or inhibit fault rupture depends not only on location but also on its strike and dip. These parameters, together with the sense of slip, control the projection of the 3D flexural stress onto normal and shear stress components. Fig. 6 shows the normal stress distribution resolved along the specific fault planes of Table 1. Each pattern corresponds to a combination of strike, dip and rake, independently of the fault location, although the trace of the representative fault is depicted for reference. The results show juxtaposed patterns of negative (compression) and positive (tensile) normal stress, typical of flexed plate states. The magnitude and sign of the bending stresses depend on the depth of observation, so we have used two different observation depths. Onshore, the stress change is calculated in the upper half of the elastic plate, at 10 km depth (fault Nos. 1, 2 and 3). Offshore, the stress is calculated in the lower half, at 35 km depth (fault Nos. 4 and 5). These depths are consistent with observations of modern seismicity, which show the seismogenic region offshore to be distinctly deeper than the region onshore (Fig. 1a). This difference also emphasizes the fact that onshore faults, like the Vilariça and Lower Tagus Valley faults, experience positive stress changes near the surface, while offshore faults, like the SWIM, experience positive stress changes at depth. The Horseshoe (No. 4) is the only offshore fault where failure at depth is inhibited by slightly increased compression. In fact, the normal stress changes resolved on any similar NE–SW thrusts in this area are very small (<0.25 MPa) no matter the observation depth. Other structures, like the Quarteira fault (No. 3), are not significantly perturbed by sea level changes because they stand near a nodal plane between positive and negative normal stress changes.

The bending stresses on a given fault are more pronounced either near the surface or near the bottom of the fault plane. This is evident from Fig. 7, which shows the distribution of the stress changes as a function of depth along two particular faults, the Lower Tagus Valley and the SWIM. On strike–slip faults such as these, the normal stress component provides a much larger contribution to the Coulomb stress change than the shear component. Bending increases the possibility of cracking leading to increased seismicity principally in the extreme regions of maximum curvature and highest strain. The largest positive Coulomb stress changes (0.25–0.75 MPa) occur in the upper 20 km along the Lower Tagus Valley fault system (onshore), while along the SWIM fault system (offshore) they are observed below 30 km. In these conditions we would expect a predominance of shallow (<20 km depth) earthquakes onshore and intermediate to deep (>30 km depth) earthquakes offshore.

All the previous models have assumed a constant T_e . The influence of a non-uniform T_e can be considered using a conceptual profile perpendicular to the continental margin. The finite element model in Fig. 8a shows the bending of an elastic plate with variable thickness (T_e varying between 20 and 45 km), across the SW Iberian margin for example, in response to 120 m of ocean loading. This simple model reflects some of the previous results regarding the stress pattern, but also demonstrates that the value of T_e away from the shoreline is not important. Thus, the flexural response to ocean loading is fundamentally determined by the elastic plate thickness at the edge of the load, i.e. along the coast line. Given the considerable uncertainty in T_e in western Iberia, we calculate the Coulomb stress changes at each fault as a function of T_e (Fig. 8b). The depth of observation is fixed at 10 km, to directly compare onshore and offshore faults at the same depth, and the stresses are averaged along strike. In addition to reinforce some of the observations made before (the opposite signs of stress onshore and offshore for instance) Fig. 8b allows us to compare the impact of ocean loading on the different faults. The Quarteira (No. 3) and Horseshoe (No. 4) faults

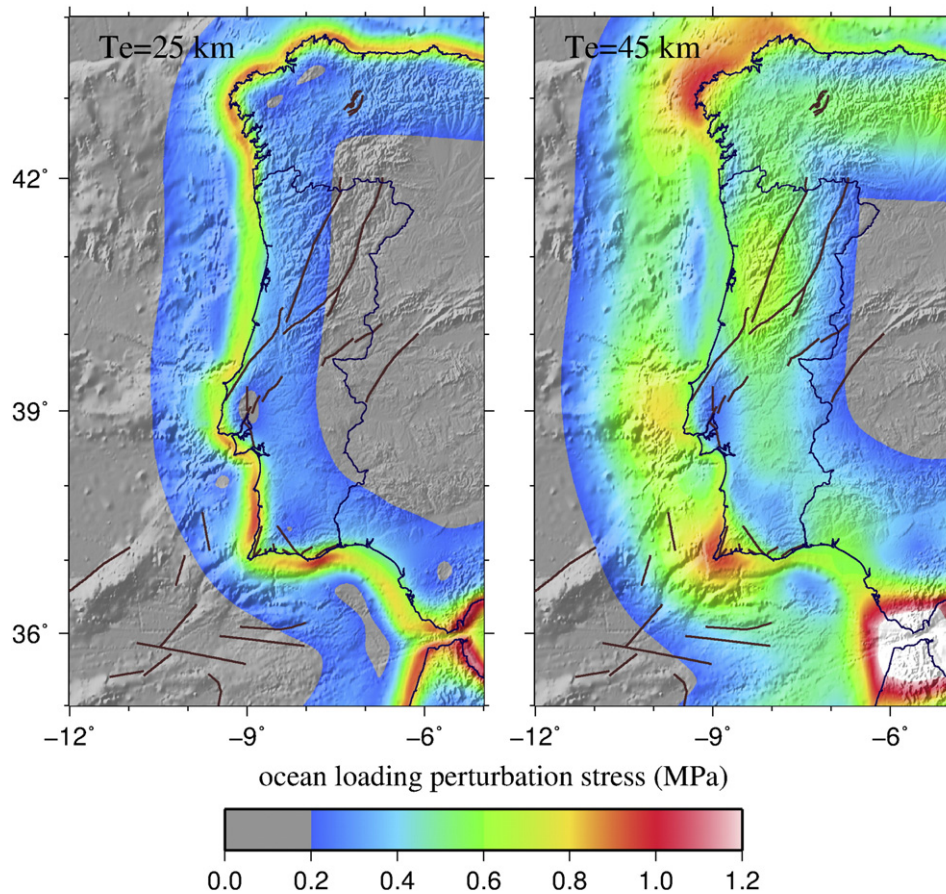


Fig. 5. Maximum shear stress due to the elastic deflection in response to 120 m of sea level rise. The stress perturbations are particularly sensitive to the elastic plate thickness (T_e) and to the geometry of the coastline. The area affected by bending is located within half a flexural wavelength of the coast, ~ 75 (150) km for $T_e = 25$ (45) km, both onshore and offshore. Ocean loading effects on faults considered in this study are more significant for large T_e (45 km) and on faults relatively away from the shoreline.

are found to be remarkably indifferent to the ocean loading perturbation effect, no matter the value of T_e . On the contrary, all the other modeled faults are favorable located/oriented to be influenced by sea level changes. A clear similarity between onshore (No. 1 and 2) and offshore faults (No. 5) becomes apparent in what regards the magnitude of the Coulomb stress changes. As expected, promotion and inhibition of failure, by positive and negative Coulomb perturbations respectively, is accentuated with increasing T_e . However, beyond $T_e = 45$ km the plate is stiff enough to resist further bending, so the Coulomb stress perturbations are limited to ± 0.5 MPa on average. It is worth mentioning that faults are obviously not planar and can experience significant variations of strike and dip. Variations in dip have been shown to have a greater influence on Coulomb stress changes than variations in strike (Luttrell and Sandwell, 2010). Changes in Coulomb stress are also highly sensitive to kinks in fault geometry. All these geometric and potentially amplifying effects are ignored in this study.

Finally, in order to explore the sensitivity of the stress perturbations to the amount of sea level rise, we compare the stress perturbations on the Vilarica region considering two distinct time spans. In addition to the total 120 m of sea level rise since the Last Glacial Maximum, Fig. 9 also shows the response to a shorter period of loading, more specifically the 5000 year period of rapid sea level rise coinciding with the cluster of events found on the Vilarica fault. A 5000 year period is still much greater than the Maxwell relaxation time of the asthenosphere (200 years) so there are no stress contributions from asthenosphere-loading interactions. The magnitude of the stress perturbations is simply directly proportional to the weight of the load, and therefore for nearly half sea level rise (~ 50 m) we obtain nearly half stress perturbations (Fig. 9). An average Coulomb

stress increase of 0.25 MPa during 5000 years corresponds to a loading rate increase of 0.05 kPa/year. This may be larger than the average tectonic loading rate in mainland Portugal given the extremely slow fault slip rates observed today (< 0.5 mm/year). In these circumstances, the sea level rise could certainly impact the seismic cycle of the Vilarica fault, bringing it closer to failure and possibly triggering the earthquake clusters.

6. Discussion

6.1. Comparison with sea level effects in other regions

The impact of eustatic sea level rise on the seismic cycle of near shore faults has originally been studied at the global scale (Luttrell and Sandwell, 2010). The stress perturbations due ocean loading were calculated at major plate boundaries, specifically, the San Andreas fault (SAF), the Alpine fault and the Cascadia subduction zone. These settings comprise fault systems that follow the coastline for hundreds to thousands of kilometers, accommodating most of the total relative motion between the adjacent plates (e.g. SAF: $\sim 80\%$; Alpine system: $\sim 75\%$). The tectonic framework of the faults in Portugal is quite different from the above in many respects. The Nubia–Eurasia plate boundary offshore southern Portugal, instead of being a typical plate boundary with a clear expression of a main fault strand, is composed by a considerable number of widespread and differently orientated active tectonic structures which accommodate the plate convergence in a diffusive way. It is estimated that the most prominent faults (the NNE–SSW to NE–SW trending thrusts and the WNW–ESE dextral strike–slip faults, represented by the Horseshoe and SWIM faults in this study) accommodate

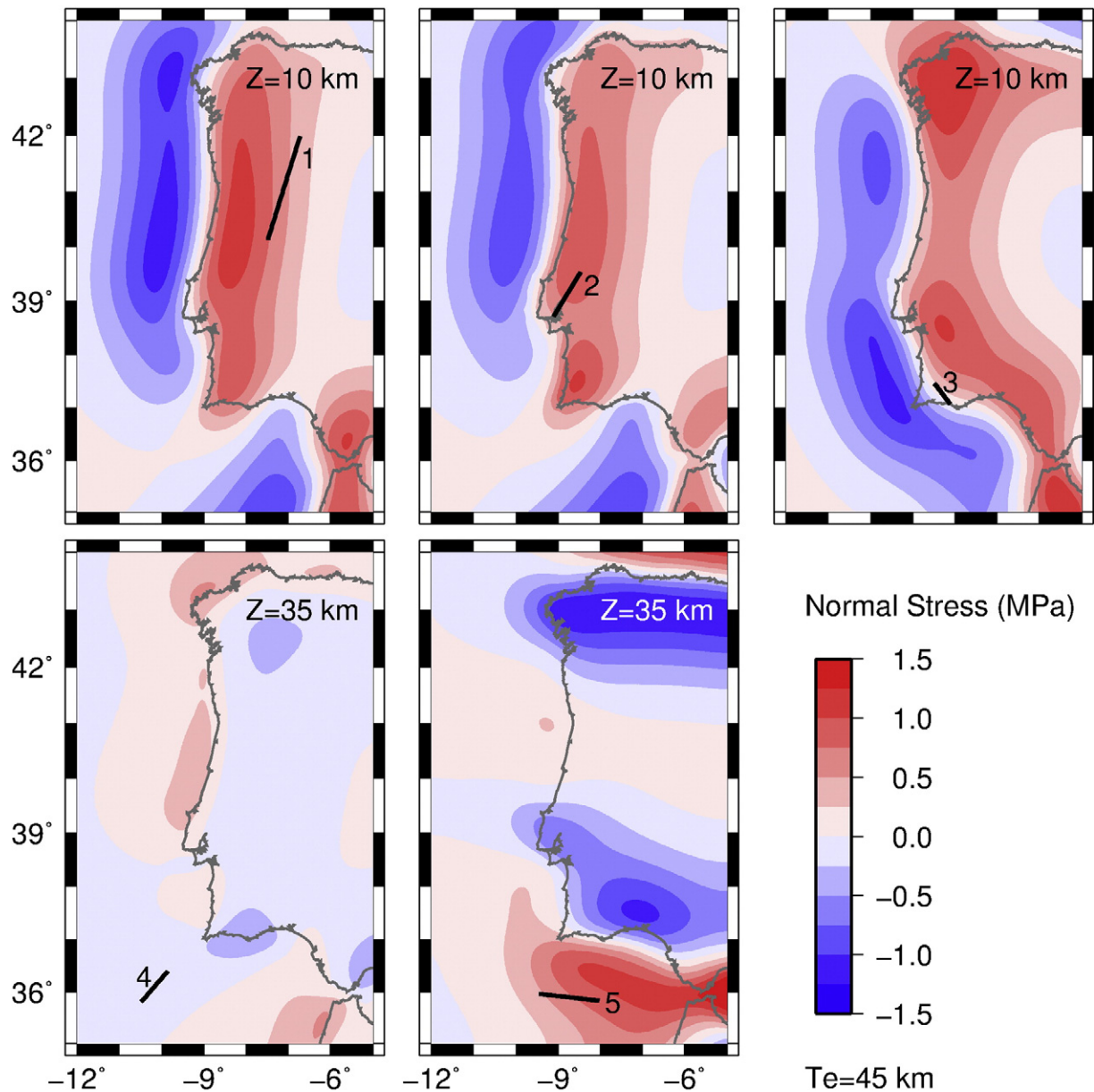


Fig. 6. Regional view of perturbations to normal stress resolved along specific fault planes (Table 1). The plate is 45 km thick in all cases but the observation depth is 10 km for onshore faults (Nos. 1, 2, 3) and 35 km for offshore faults (Nos. 4, 5), above and below the neutral surface, respectively. Positive normal stresses (red) correspond to tension and negative (blue) to compression. The regional normal stress perturbations on nearly vertical faults (all except fault No. 4) follow the coastline coinciding with the flexural bulge onshore and flexural moat offshore.

only ~50% of the average plate relative motion and slip at rates of no more than 1–2 mm/year (e.g. Cunha et al., 2012; Rosas et al., 2012). Towards the continent, the rate of deformation decreases with increasing distance from the plate boundary, as evidenced by estimates of inter-seismic strain accumulation derived from GPS data (Neves et al., 2014; Stich et al., 2006). At the present time, the northern region of mainland Portugal is a very slowly straining region with estimated fault slip rates of less than 0.5 mm/year, in strong contrast with the aforementioned plate boundary fault systems analyzed in previous studies.

As the climatic forcing is independent of the tectonic setting it comes as no surprise that the stress perturbations due to the eustatic sea level rise are similar in all of the analyzed regions. In fact, the Coulomb stress changes induced in the SAF and Alpine faults, varying between 0.5 and 1 MPa, are nearly identical to the Coulomb stress changes computed for some of the faults in Portugal, namely the Vilarica, LTV and SWIM faults. The key point to consider, thus, is the relative difference between

the Coulomb stress changes due to sea level rise and the stress accumulation rate due to tectonic forcing. For instance, in the SAF a fault slip rate of 4–40 mm/year is estimated to correspond to a tectonic loading rate of 5–125 kPa/year (Smith and Sandwell, 2003). When compared to the tectonic loading rate the Coulomb stress change due to the sea level rise (0.1 kPa/year or 1 MPa in 10,000 years) increases at a much lower rate (10–1000 times less). For this reason, it has been recognized that ocean loading effects are unlikely to be noticed on southern California faults. Following the same line of reasoning a fault slip rate of ~0.4 mm/year in Portugal corresponds to a tectonic loading rate of ~0.5 kPa/year, which is of the same order of magnitude as the Coulomb stress change rate due to sea level rise. In this case, ocean loading may substantially affect the long-term Coulomb stress accumulation rate, confirming that faults in Portugal are more likely to have been perturbed by sea level rise than faults in California, or in other major plate boundary regions.

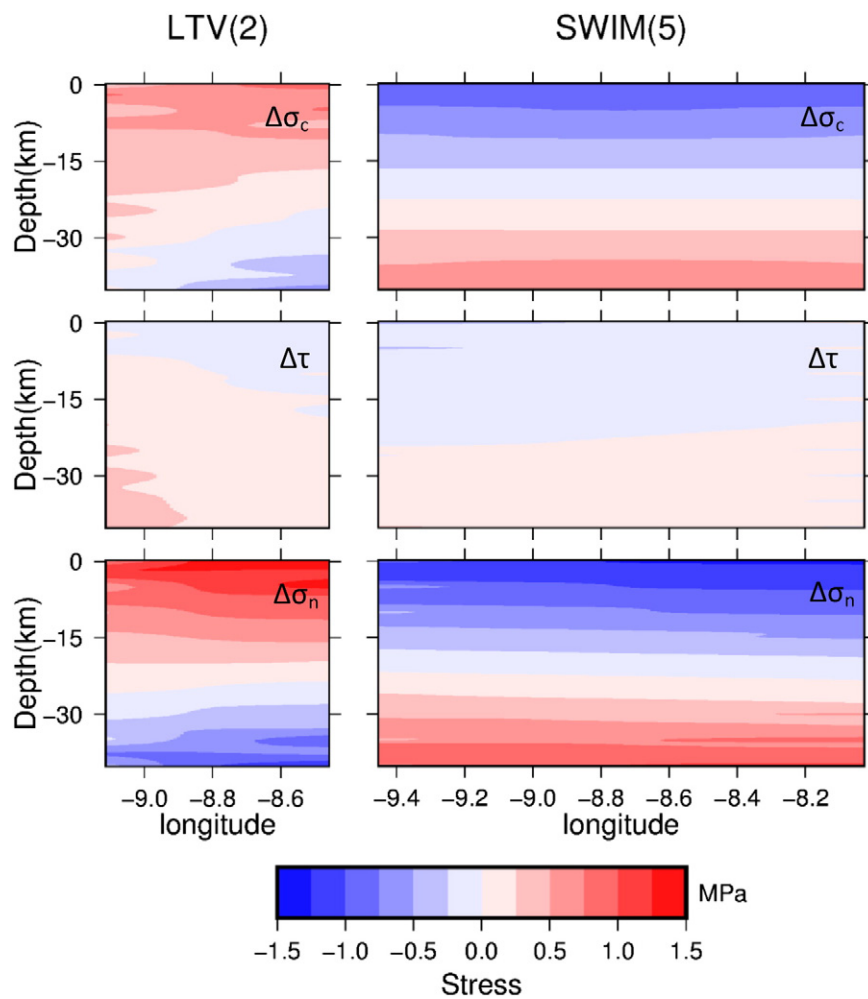


Fig. 7. Distribution of the normal ($\Delta\sigma_n$), shear ($\Delta\tau$) and Coulomb ($\Delta\sigma_c$) stress changes as a function of depth (for $T_e = 45$ km), resolved along the Lower Tagus Valley (No. 2) and SWIM (No. 5) fault planes. Ocean loading effects promote failure ($\Delta\sigma_c > 0$) at shallow levels onshore and at large depths offshore.

6.2. Implications for seismic activity in Portugal

The connection between variations in seismicity rates and sea level changes has not yet been proven. There is no sufficient available evidence anywhere in the world, paleoseismic data or indirect indicators, demonstrating the existence of periodic variation in earthquake frequency synchronous with Milankovitch climate oscillations. In Portugal, given the slow deformation rates, infrequent large earthquakes and long recurrence times, this relation is very difficult to prove. We would need very long paleoseismic records, with enough resolution to distinguish events and, especially, abundant enough to be statistically significant. One of the merits of studies like this one is to recognize the feasibility of this hypothesis and stimulate further research on climate and tectonic interactions. In this perspective, our models help to motivate future field work since we were able to identify which faults will more likely possess a paleoseismic record of ocean loading effects.

The detection of ocean loading effects depends on the relation between fault reactivation potential, due to ongoing tectonic processes, and Coulomb stress changes induced by sea level changes. In mainland Portugal, the slip tendency analysis shows that the Vilarica and LTV faults have a low potential of reactivation under present tectonic loading. In the LTV fault it has been estimated that M 6–7 characteristic earthquakes occur in clusters, separated by recurrence times of the order of 2000–5000 years (Carvalho et al., 2006). Earthquake recurrence intervals of thousands of years (2 ka) have also been proposed for the

Vilarica fault (Rockwell et al., 2009). Our flexural models show that over a seismic cycle of 2000 years, for example, the Coulomb stress changes induced by sea level rise is 0.1–0.5 MPa in both the Vilarica and LTV faults. These stress changes may be able to trigger earthquakes if the faults are already close to failure. Uncertainties in fault parameters, such as dip angle and friction coefficient, are second order relative to the effects of elastic plate thickness and fault location relative to the coastline. Moreover, while geometrical effects have been ignored by embedding straight faults in the models, more complicated simulations have shown high rates of stress at fault bends and kinks (Smith and Sandwell, 2004), which suggest that more realistic fault geometries would yield even higher Coulomb stress changes. Hence, it may be possible to find a causal relationship between sea level change and fault rupture in these two faults. Based on the pattern of the ocean loading perturbation stress (Fig. 5, $T_e = 45$ km) we suggest that other suitable faults to search for paleoseismic evidence related to sea level rise are the Penacova–Régua–Verin and the Nazaré–Caldas da Rainha–Vimeiro faults (at similar latitudes but closer to the coastline). Another fault system that is affected by positive Coulomb stress changes due to sea level rise (results not shown) is the Teotónio–Aljezur–Sincera fault system, in south Portugal. A small increase in the rate of fault activity during the Pleistocene, inferred along the northern segments of this fault (Figueiredo, 2015), is possibly related to ocean loading effects.

In contrast with the above, the Quarteira and Horseshoe faults have intermediate to high fault slip tendency at present stress conditions, but display no sensitivity to ocean loading effects. Future paleoseismic

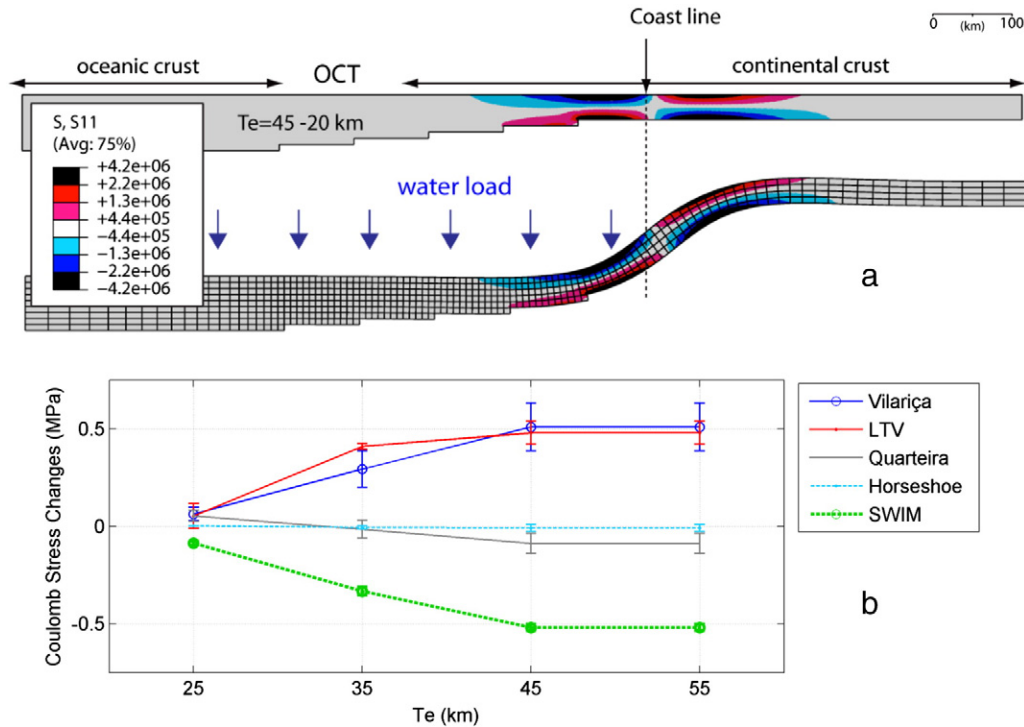


Fig. 8. (a) Model of bending along a conceptual profile perpendicular to western Iberia margin. OCT denotes ocean/continent transition. The elastic plate thickness (T_e) varies between 45 (offshore) and 20 km (onshore). The stress pattern is mainly determined by the value of the elastic thickness at the edge of the oceanic load (coast line). (b) Dependence of the Coulomb stress change on the elastic plate thickness. The Coulomb stress changes resolved at each fault are calculated for a common observation depth of 10 km and averaged along strike.

research that may eventually be conducted on the Quarteira fault may not find any linkages to eustatic sea level rise. Likewise, the Horseshoe fault is not expected to show any change in earthquake frequency or recurrence time linked to ocean loading. This and other NE–SW thrusts in the area owe their seismicity to regular tectonic earthquake cycle factors and are probably just as much a hazard today as they have been throughout the Pleistocene–early Holocene. Nonetheless, as the preservation of records of late Pleistocene seismic activity is expected to be better in the marine environment, future work focusing on the relation between rising sea level and offshore paleoseismic evidence (e.g. mass transport deposits and turbidites) will help to clarify this issue.

7. Conclusions

The potential of reactivation of the set of active faults analyzed in this study, measured in terms of normalized slip tendency (T_s), varies across Portugal and depends mainly on the fault's orientation relative to the current regional stress field. In the northern and central parts of the territory, the NNE–SSW left-lateral strike–slip fault systems, represented here by the Vilarica and Lower Tagus Valley faults, have a low potential of reactivation ($T_s < 0.5$). Our results support the notion that these faults are on average characterized by low rates of stress accumulation (< 0.5 kPa/year) and long recurrence times (> 1000 years) for high magnitude earthquakes. In the south of Portugal, the Quarteira fault is favorably oriented for reactivation ($T_s \sim 0.8$). Although large superficial fault ruptures remain to be identified in the field, this fault may be accumulating significant stress at depth, which makes it a major potential source of damaging earthquakes in the Algarve region. The faults with the largest potential of reactivation ($T_s \sim 1.0$) are the NNE–SSW trending thrusts offshore SW Iberia, such as the Horseshoe fault. There is a good correlation between slip tendency and fault activity, as most of the earthquakes that occur in Portugal are concentrated along these structures.

The flexural effects of ocean loading in Portugal, and the consequent perturbations of the stress field, have been evaluated for a sea level rise of ~ 120 m since the Last Glacial Maximum. The most intense stress perturbations are shown to occur in the corner regions of west Iberia (Cape Finisterre and Cape St. Vicente), assuming an elastic plate thickness of 45 km. Positive Coulomb stress changes, that can favor fault rupture, are predicted at shallow depths (< 20 km) onshore, and at great depths (> 30 km) offshore. The Coulomb stress changes calculated along the Quarteira and the Horseshoe faults are extremely small, independently of the elastic plate thickness. We conclude that these faults are completely unaffected by flexural effects related to sea level changes, and hence, are unlikely to possess any paleoseismic record of this phenomenon. In contrast, Coulomb stress increases of 0.5 MPa, on average, are predicted for the Vilarica and Lower Tagus Valley faults. This is estimated to be of the same order of magnitude as the Coulomb stress accumulation due to regular tectonic loading. Therefore, sea level rise is capable of impacting the seismic cycle of the Vilarica fault, bringing it closer to failure and possibly triggering the earthquake clusters that have been observed over there. Our results confirm that the ideal faults to pursue further paleoseismic research regarding the effects of sea level changes in Portugal are the Vilarica and the Lower Tagus Valley fault systems.

In summary, the effects of sea level changes can be significant in Portugal, especially in faults with favorable location, geometry and kinematics. It is reasonable to presume that the Pleistocene seismic cycles on these faults could have been partially controlled by sea level oscillations and consequently, climate induced effects should be considered in future seismic hazard analysis.

Acknowledgments

The authors acknowledge IDL and FCT for supporting this work through project FASTLOAD (PTDC/GEO-GEO/2860/2012). We thank D. Brothers and J. Carvalho for their constructive and thorough reviews of the manuscript.

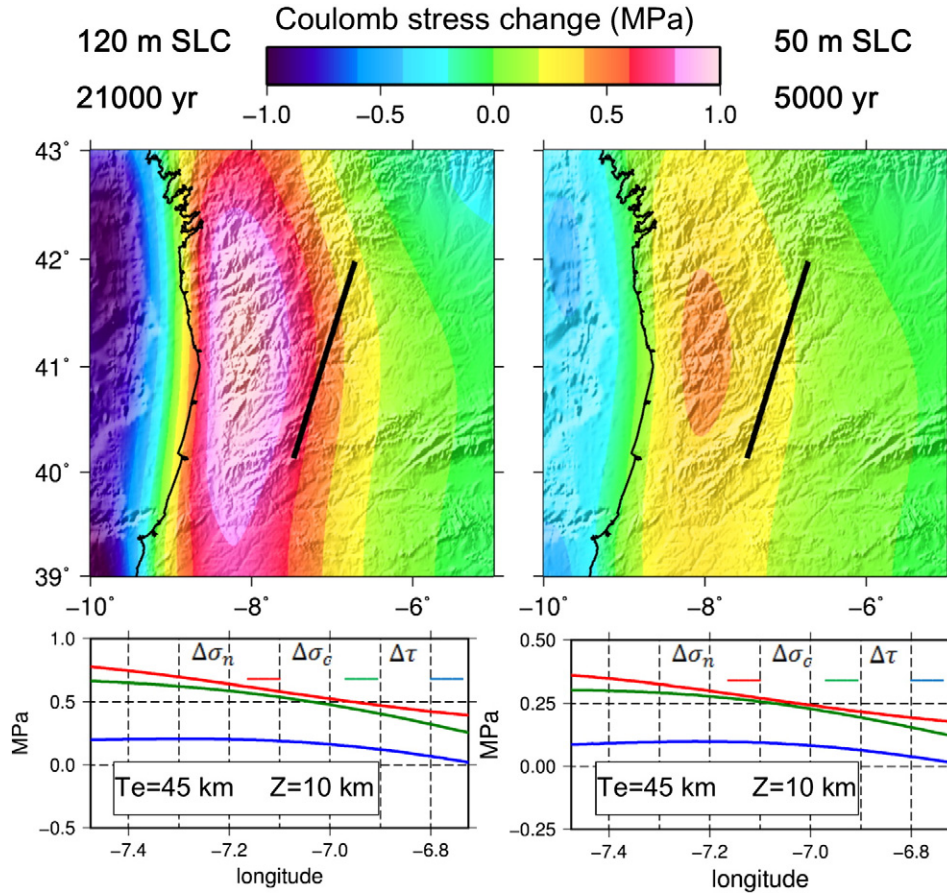


Fig. 9. Stress perturbation in the Vilarica region for two different amounts/durations of sea level change (SLC). Normal ($\Delta\sigma_n$), shear ($\Delta\tau$) and Coulomb ($\Delta\sigma_c$) stress changes resolved on the Vilarica fault are displayed along strike. The stress changes are directly proportional to the amount of loading but are otherwise not affected by the loading rate. Strike-slip faults subparallel to the Vilarica and closer to the shoreline may experience Coulomb stress changes of up to 1 MPa.

Appendix A

The slip tendency analysis relies on the widely used Wallace–Bott hypothesis which states that the direction of movement after a fracture is formed coincides with the direction of maximum shearing stress within the fracture plane. Although the validity of this hypothesis may be questioned, for it presupposes the homogeneity of the stress state and neglects factors such as fault interaction and fault block rotation, several studies demonstrated that it can be used as a first order approximation for the prediction of fault slip (Neves et al., 2009 and references therein).

If we know the stress tensor completely (principal stress directions and principal stress values) the shear and normal stresses, τ and σ , acting on a given plane are simply (Jaeger, 1969),

$$\tau^2 = (\sigma_1 - \sigma_2)^2 l^2 m^2 + (\sigma_2 - \sigma_3)^2 m^2 n^2 + (\sigma_3 - \sigma_1)^2 n^2 l^2 \quad (1)$$

$$\sigma = l^2 \sigma_1 + m^2 \sigma_2 + n^2 \sigma_3 \quad (2)$$

where σ_i ($i = 1, 2, 3$) are the principal stress values and (l, m, n) are the direction cosines of the normal to the plane in the principal stress system. Most commonly, however, we only know the principal stress directions and the principal stress difference ratio, $R = (\sigma_1 - \sigma_2) / (\sigma_1 - \sigma_3)$.

Using the shape ratio ϕ definition,

$$\phi = 1 - R = (\sigma_2 - \sigma_3) / (\sigma_1 - \sigma_3) \quad (3)$$

the principal stress values can be rewritten in terms of ϕ and two unknown parameters k_1 and k_2 , related to the size and location of the three-dimensional Mohr circles (Neves et al., 2009),

$$\sigma_1 = k_1 + k_2 \quad (4)$$

$$\sigma_2 = k_1 \phi + k_2 \quad (5)$$

$$\sigma_3 = k_2. \quad (6)$$

Upon substitution of these expressions in the criterion for frictional sliding ($\mu = \tau / \sigma$), and using the identity $\tan \varphi = 1 / \tan 2\theta$, it can be shown that,

$$k_2 = k_1 \csc \varphi - \sigma_1 \quad (7)$$

and the parameter k_2 can be eliminated from the principal stress value equations. This allows rewriting the shear and normal stress acting on a given plane as,

$$\tau = k_1 \left[(1 - \phi)^2 l^2 m^2 + \phi^2 m^2 n^2 + n^2 l^2 \right]^{1/2} \quad (8)$$

$$\sigma = k_1 \left(\frac{\csc \varphi + 1}{2} - (1 - \phi) m^2 - n^2 \right). \quad (9)$$

It follows that the slip tendency T_s computed from these expressions is independent of the choice of the unknown parameter k_1 . Thus, the relative magnitude of the shear and normal stresses (slip tendency) is

independent of the absolute magnitude of the principal stresses and only depends on the orientation of the fracture plane in the stress field and on the principal stress difference ratio.

References

- Baptista, M.A., Miranda, J.M., Chierici, F., Zitellini, N., 2003. New study of the 1755 earthquake source based on multi-channel seismic survey data and tsunami modeling. *Nat. Hazards Earth Syst. Sci.* 3, 333–340. <http://dx.doi.org/10.5194/nhess-3-333-2003>.
- Baptista, M.A., Miranda, J.M., Lopes, F.C., Luis, J.F., 2007. The source of the 1722 Algarve earthquake: evidence from MCS and Tsunami data. *J. Seismol.* 11, 371–380.
- Bartolome, R., Gràcia, E., Stich, D., Martínez-Lorientte, S., Klaeschen, D., Mancilla, F.L., Iacono, C.L., Dañoibeitia, J.J., Zitellini, N., 2012. Evidence for active strike–slip faulting along the Eurasia–Africa convergence zone: implications for seismic hazard in the southwest Iberian margin. *Geology* 40 (6), 495–498.
- Becker, J.J., Sandwell, D.T., Smith, W.H.F., Braud, J., Binder, B., Depner, J., Fabre, D., Factor, J., Ingalls, S., Kim, S.-H., Ladner, R., Marks, K., Nelson, S., Pharaoh, A., Trimmer, R., Von Rosenberg, R., Wallace, G., Weatherall, P., 2009. Global bathymetry and elevation data at 30 arc seconds resolution: SRTM30 PLUS. *Mar. Geod.* 32 (4), 355–371.
- Bettinelli, P., Avouac, J.P., Flouzat, M., Bollinger, L., Ramillien, G., Rajaure, S., Sapkota, S., 2008. Seasonal variations of seismicity and geodetic strain in the Himalaya induced by surface hydrology. *Earth Planet. Sci. Lett.* 266 (3–4), 332–344. <http://dx.doi.org/10.1016/j.epsl.2007.11.021>.
- Bollinger, L., Perrier, F., Avouac, J.P., Sapkota, S., Gautam, U., Tiwari, D.R., 2007. Seasonal modulation of seismicity in the Himalaya of Nepal. *Geophys. Res. Lett.* 34, L08304. <http://dx.doi.org/10.1029/2006GL029192>.
- Borges, J.F., Fitas, A.J.S., Bezzeghoud, M., Teves-Costa, P., 2001. Seismotectonics of Portugal and its adjacent Atlantic area. *Tectonophysics* 337, 373–387.
- Brothers, D., Kilb, D., Luttrell, K., Driscoll, N., Kent, G., 2011. Loading of the San Andreas fault by flood-induced rupture of faults beneath the Salton Sea. *Nat. Geosci.* 4, 486–492. <http://dx.doi.org/10.1038/ngeo1184>.
- Brothers, D.S., Luttrell, K.M., Chaytor, J.D., 2013. Sea-level-induced seismicity and submarine landslide occurrence. *Geology* 41, 979–982. <http://dx.doi.org/10.1130/G34410.1>.
- Byerlee, J.D., 1978. Friction of rocks. *Pure Appl. Geophys.* 102, 453–475.
- Cabral, J., 1989. An example of intraplate neotectonic activity, Vilarica basin, northeast Portugal. *Tectonics* 8 (2), 285–303.
- Cabral, J., 1995. Neotectónica em Portugal Continental. 31. *Memórias do Instituto Geológico e Mineiro* (265 pp.).
- Cabral, J., 2012. Neotectonics of mainland Portugal: state of the art and future perspectives. *J. Iber. Geol.* 38 (1), 71–84.
- Cabral, J., Moniz, C., Ribeiro, P., Terrinha, P., Matias, L., 2003. Analysis of seismic reflection data as a tool for the seismotectonic assessment of a low activity intraplate basin in the Lower Tagus Valley (Portugal). *J. Seismol.* 7, 431–447.
- Cabral, J., Moniz, C., Batlló, J., Figueiredo, P., Carvalho, J., Matias, L., Teves-Costa, P., Dias, R., Simão, N., 2013. The 1909 Benavente (Portugal) earthquake: search for the source. *Nat. Hazards* 69, 1211–1227.
- Carvalho, J., Cabral, J., Gonçalves, R., Torres, L., Mendes-Victor, L., 2006. Geophysical methods applied to fault characterization and earthquake potential assessment in the Lower Tagus Valley, Portugal. *Tectonophysics* 418, 277–297.
- Carvalho, J., Matias, H., Rabeh, T., Menezes, P.T.L., Barbosa, V.C.F., Dias, R., Carrilho, F., 2012. Connecting onshore structures in the Algarve with the southern Portuguese continental margin: the Carcavai fault zone. *Tectonophysics* 570, 151–162.
- Carvalho, J., Rabeh, T., Dias, R., Pinto, C., Oliveira, T., Cunha, T., Borges, J., 2014. Tectonic and neotectonic implications of a new basement map of the Lower Tagus Valley, Portugal. *Tectonophysics* 617, 88–100.
- Cloetingh, S., Burrov, E., Beekman, F., Andeweg, B., Andriessen, P.A.M., Garcia-Castellanos, D., de Vicente, G., Vegas, R., 2002. Lithospheric folding in Iberia. *Tectonics* 21 (5), 1041.
- Colletini, C., 2011. The mechanical paradox of low-angle normal faults: current understanding and open questions. *Tectonophysics* 510, 253–268.
- Crouch, S.L., Starfield, A.M., 1983. *Boundary Element Methods in Solid Mechanics*. Allen & Unwin, London (322 pp.).
- Cunha, T.A., Watts, A.B., Pinheiro, L.M., Myklebust, R., 2010. Seismic and gravity anomaly evidence of large-scale compressional deformation off SW Portugal. *Earth Planet. Sci. Lett.* 293, 171–179.
- Cunha, T.A., Matias, L.M., Terrinha, P., Negrodo, A., Rosas, F., Fernandes, R.M.S., Pinheiro, L.M., 2012. Neotectonics of the SW Iberia margin, Gulf of Cadiz and Alboran Sea: a reassessment including recent structural, seismic and geodetic data. *Geophys. J. Int.* 188, 850–872.
- de Vicente, G., Cloetingh, S., Muñoz-Martín, A., Olaiz, A., Stich, D., Vegas, R., Fernández-Lozano, J., 2008. Inversion of moment tensor focal mechanisms for active stresses around the microcontinent Iberia: tectonic implications. *Tectonics* 27 (1), 1–22.
- Dias, R.P., 2001. Neotectónica da Região do Algarve (PhD dissertation) Universidade de Lisboa, Portugal.
- Duarte, J.C., Rosas, F.M., Terrinha, P., Shellart, W.P., Boutelier, D., Gutscher, M.-A., Ribeiro, A., 2013. Are subduction zones invading the Atlantic? Evidence from the southwest Iberia margin. *Geology* 41, 839–842.
- Fairbanks, R.G., 1989. A 17,000 year glacial eustatic sea level record: influence of glacial melting rates on the Younger Dryas event and deep ocean circulation. *Nature* 342, 637–641.
- Figueiredo, P.M., 2015. Neotectonics of SW Portugal. Implications for seismic hazard knowledge (PhD dissertation) Universidade de Lisboa, Portugal.
- Gahalaut, K., Gahalaut, V.K., Pandey, M.R., 2007. A new case of reservoir triggered seismicity: Govind Ballav Pant reservoir (Rihand dam), central India. *Tectonophysics* 439 (1–4), 171–178. <http://dx.doi.org/10.1016/j.tecto.2007.04.003>.
- García-Orellana, J., Gràcia, E., Vizcaino, A., Masqué, P., Olib, C., Martínez-Ruiz, F., Pineró, E., Sanchez-Cabeza, J.A., Danõibeitia, J.J., 2006. Identifying instrumental and historical earthquake records in the SW Iberian Margin using ²¹⁰Pb turbidite chronology. *Geophys. Res. Lett.* 33, 24. <http://dx.doi.org/10.1029/2006GL028417>.
- Geissler, W.H., Matias, L., Stich, F., Carrilho, F., Jokat, W., Monna, S., IbenBrahim, A., Mancilla, F., Gutscher, M.A., Sallarès, V., Zitellini, N., 2010. Focal mechanisms for sub-crustal earthquakes in the Gulf of Cadiz from a dense OBS deployment. *Geophys. Res. Lett.* 37, L18309.
- Gómez-Ortiz, D., Tejero, R., Ruiz, J., Babin-Vich, R., Gonzalez-Casado, J.M., 2005. Estimating the effective elastic thickness of the lithosphere of the Iberian Peninsula based on multitaper spectral analysis. *Geophys. J. Int.* 160, 729–735.
- Gràcia, E., Danõibeitia, J., Vergés, J., Córdoba, D., PARSIFAL Team, 2003. Mapping active faults offshore Portugal (36°N–38°N): implications for seismic hazard assessment along the southwest Iberian margin. *Geology* 31 (1), 83–86.
- Gràcia, E., Vizcaino, A., Escutia, C., Asioli, A., Rodés, A., Pallás, R., García-Orellana, J., Lebreiro, S., Goldfinger, C., 2010. Holocene earthquake record offshore Portugal (SW Iberia): testing turbidite paleoseismology in a slow-convergence margin. *Quat. Sci. Rev.* 29, 1156–1172.
- Grollimund, B., Zoback, M.D., 2000. Post glacial lithospheric flexure and induced stresses and pore pressure changes in the northern North Sea. *Tectonophysics* 327 (1–2), 61–81.
- Heki, K., 2001. Seasonal modulation of interseismic strain buildup in northeastern Japan driven by snow loads. *Science* 293, 89–92.
- Hetzl, R., Hampel, A., 2005. Slip rate variations on normal faults during glacial-interglacial changes in surface loads. *Nature* 435 (7038), 81–84.
- Jaeger, J.C., 1969. *Elasticity, Fracture and Flow with Engineering and Geological Applications*. 1st ed. Methuen & Co. Ltd., London (268 pp.).
- Kaufmann, G., Amelung, F., 2000. Reservoir-induced deformation and continental rheology in vicinity of Lake Mead, Nevada. *J. Geophys. Res. Solid Earth* 105 (B7), 16341–16358.
- King, G., Stein, R., Lin, J., 1994. Static stress changes and the triggering of earthquakes. *Bull. Seismol. Soc. Am.* 84, 935–953.
- Lambeck, K., Rouby, H., Purcell, A., Sun, Y., Sambridge, M., 2014. Sea level and global ice volumes from the Last Glacial Maximum to the Holocene. *Proc. Natl. Acad. Sci.* 111 (43), 15296–15303.
- Lin, J., Stein, R.S., 2004. Stress triggering in thrust and subduction earthquakes and stress interaction between the southern San Andreas and nearby thrust and strike–slip faults. *J. Geophys. Res. Solid Earth* 109, B02303. <http://dx.doi.org/10.1029/2003JB002607>.
- Luttrell, K., Sandwell, D., 2010. Ocean loading effects on stress at near shore plate boundary fault systems. *J. Geophys. Res. Solid Earth* 115, B08411. <http://dx.doi.org/10.1029/2009JB006541>.
- Luttrell, K., Sandwell, D., Smith-Konter, B., Bills, B., Bock, Y., 2007. Modulation of the earthquake cycle at the southern San Andreas fault by lake loading. *J. Geophys. Res. Solid Earth* 112, B08411. <http://dx.doi.org/10.1029/2006JB004752>.
- Martínez-Lorientte, S., Sallarès, V., Gràcia, E., Bartolome, R., Dañoibeitia, J.J., Zitellini, N., 2014. Seismic and gravity constraints on the nature of the basement in the Africa–Eurasia plate boundary: new insights for the geodynamic evolution of the SW Iberian margin. *J. Geophys. Res. Solid Earth* 119, 127–149. <http://dx.doi.org/10.1002/2013JB010476>.
- Matias, L.M., Cunha, T., Annunziato, A., Baptista, M.A., Carrilho, F., 2013. Tsunamiogenic earthquakes in the Gulf of Cadiz: fault model and recurrence. *Nat. Hazards Earth Syst. Sci.* 13, 1–13.
- Middleton, T.A., Copley, A., 2014. Constraining fault friction by re-examining earthquake nodal plane dips. *Geophys. J. Int.* 196 (2), 671–680. <http://dx.doi.org/10.1093/gji/ggt427>.
- Morris, A., Ferril, D.A., Henderson, D.B., 1996. Slip-tendency analysis and fault reactivation. *Geology* 24, 275–278.
- Neves, M.C., Paiva, L.T., Luis, J., 2009. Software for slip-tendency analysis in 3D: a plug-in for Coulomb. *Comput. Geosci.* 35, 2345–2352.
- Neves, M.C., Fernandes, R.M., Adam, C., 2014. Refined models of gravitational potential energy compared with stress and strain rate patterns in Iberia. *J. Geodyn.* 81, 91–104.
- Okada, Y., 1992. Internal deformation due to shear and tensile faults in a half-space. *Bull. Volcanol.* 47, 239–246.
- Peltier, W.R., Fairbanks, R.G., 2006. Global glacial ice volume and Last Glacial Maximum duration from an extended Barbados sea level record. *Quat. Sci. Rev.* 25, 3322–3337.
- Pereira, H., Cabral, J., Figueiredo, P.M., Besana-Ostman, G.M., Brum da Silveira, A., Cunha, P.P., Gomes, A., Lopes, F.C., Pereira, D., Rockwell, T., 2010. Actividade sísmica quaternária da falha da Vilarica (NE Portugal): resultados preliminares de um estudo paleossismológico. *e-Terra* 11 (6) (<http://metododirecto.pt/CNG2010/index.php/vol/article/view/279/0>).
- Pérez-Gussinyé, M., Watts, A.B., 2005. The long-term strength of Europe and its implications for plate-forming processes. *Nature* 436, 381–384.
- Pinheiro, L.M., Whitmarsh, R.B., Miles, P.R., 1992. The ocean-continent boundary off the western continental margin of Iberia-II. Crustal structure in the Tagus Abyssal Plain. *Geophys. J. Int.* 109, 106–124.
- Pro, C., Buforn, E., Bezzeghoud, M., Udias, A., 2013. Mechanism of 2003, 2007 and 2009 earthquakes (S. Vicente Cape) and implications for the 1755 Lisbon earthquake. *Tectonophysics* 583, 16–27.
- Ribeiro, A., Cabral, J., Baptista, R., Matias, L., 1996. Stress pattern in Portugal mainland and the adjacent Atlantic region, West Iberia. *Tectonics* 15 (2), 641–659.
- Rockwell, T., Fonseca, J., Madden, C., Dawson, T., Owen, L.A., Vilanova, S., Figueiredo, P., 2009. Paleoseismology of the Vilarica Segment of the Manteigas–Bragança Fault in Northeastern Portugal. In: Reicherter, K., Michetti, A.M., Silva, P.G. (Eds.),

- Palaeoseismology: historical and prehistorical records of earthquake ground effects for seismic hazard assessment. *Geol. Soc. London, London*, pp. 237–258.
- Rosas, F.M., Duarte, J.C., Terrinha, P., Valadares, V., Matias, L., 2009. Morphotectonic characterization of major bathymetric lineaments in Gulf of Cadiz (Africa–Iberia plate boundary): insights from analogue modeling experiments. *Mar. Geol.* 261, 33–47.
- Rosas, F.M., Duarte, J.C., Neves, M.C., Terrinha, P., Silva, S., Matias, L., 2012. Thrust–wrench interference between major active faults in the Gulf of Cadiz (Africa–Eurasia plate boundary, offshore SW Iberia): tectonic implications from analogue and numerical modeling. *Tectonophysics* 548–549, 1–21.
- Sallarès, V., Martínez-Loriente, S., Prada, M., Gràcia, E., Ranero, C.R., Gutscher, M.-A., Bartolome, R., Gailler, A., Dañobeitia, J.J., Zitellini, N., 2013. Seismic evidence of exhumed mantle rock basement at the Gorringe Bank and the adjacent Horseshoe and Tagus abyssal plains (SW Iberia). *Earth Planet. Sci. Lett.* 365, 120–131.
- Simpson, D.W., Leith, W.S., Scholz, C.H., 1988. Two types of reservoir-induced seismicity. *Bull. Seismol. Soc. Am.* 78 (6), 2025–2040.
- Smith, B., Sandwell, D., 2003. Coulomb stress accumulation along the San Andreas Fault system. *J. Geophys. Res. Solid Earth* 108 (B6), 2296. <http://dx.doi.org/10.1029/2002JB002136>.
- Smith, B., Sandwell, D., 2004. A three-dimensional semianalytic viscoelastic model for time-dependent analyses of the earthquake cycle. *J. Geophys. Res. Solid Earth* 109, B12401. <http://dx.doi.org/10.1029/2004JB003185>.
- Stanford, J.D., Rohling, E.J., Hunter, S.E., Roberts, A.P., Rasmussen, S.O., Bard, E., McManus, J., Fairbanks, R.G., 2006. Timing of meltwater pulse 1a and climate responses to meltwater injections. *Paleoceanography* 21 (4), 4103.
- Steer, P., Simoes, M., Cattin, R., Shyu, J.B.H., 2014. Erosion influences the seismicity of active thrust faults. *Nat. Commun.* 5, 5564. <http://dx.doi.org/10.1038/ncomms5564>.
- Stein, R.S., 1999. The role of stress transfer in earthquake occurrence. *Nature* 402, 605–609.
- Stich, D., Batlló, J., Macià, R., Teves-Costa, P., Morales, J., 2005. Moment tensor inversion with single-component historical seismograms: the 1909 Benavente (Portugal) and Lambesc (France) earthquakes. *Geophys. J. Int.* 162, 850–858.
- Stich, D., Serpelloni, E., Mancilla, F.L., Morales, J., 2006. Kinematics of the Iberia–Maghreb plate contact from seismic moment tensors and GPS observations. *Tectonophysics* 426, 295–317.
- Terrinha, P., Pinheiro, L.M., Henriët, J.-P., Matias, L., Ivanov, M.K., Monteiro, J.H., Akhmetzhanov, A., Volkonskaya, A., Cunha, T., Shaskin, P., Rovere, M., TTR10 Shipboard Scientific Party, 2003. Tsunamigenic–seismogenic structures, neotectonics, sedimentary process and slope instability on the southwest Portuguese margin. *Mar. Geol.* 195 (1–4), 55–73.
- Terrinha, P., Matias, L., Vicente, J., Duarte, J., Luis, J., Pinheiro, L., Lourenço, N., Diez, S., Rosas, F., Magalhães, V., Valadares, V., Zitellini, N., Roque, C., Victor, L.M., Team M.A.T.E.S.P.R.O., 2009. Morphotectonics and strain partitioning at the Iberia–Africa plate boundary from multibeam and seismic reflection data. *Mar. Geol.* 267 (3–4), 156–174.
- Tesauro, M., Kaban, M.K., Cloetingh, S.A.P.L., 2012. Global strength and elastic thickness of the lithosphere. *Glob. Planet. Chang.* 90, 51–57.
- Teves-Costa, P., Rio, I., Marreiros, C., Ribeiro, R., Borges, J.F., 1999. Source parameters of old earthquakes: semi-automatic digitalization of analog records and seismic moment assessment. *Nat. Hazards* 19, 205–220.
- Toda, S., Stein, R.S., Richards-Dinger, K., Bozkurt, S., 2005. Forecasting the evolution of seismicity in southern California: animations built on earthquake stress transfer. *J. Geophys. Res. Solid Earth* B05S16 <http://dx.doi.org/10.1029/2004JB003415>.
- Vilanova, S.P., Fonseca, J.F.B.D., 2007. Probabilistic Seismic-Hazard Assessment for Portugal. *Bull. Seismol. Soc. Am.* 97 (5), 1702–1717. <http://dx.doi.org/10.1785/0120050198>.
- Vizcaino, A., Gràcia, E., Pallàs, R., Garcia-Orellana, J., Escutia, C., Casas, D., Willmott, V., Diez, S., Asioli, A., Dañobeitia, J.J., 2006. Sedimentology, physical properties and ages of mass-transport deposits associated to the Marquês de Pombal Fault, Southwest Portuguese Margin. *Nor. J. Geol.* 86, 177–186.
- Zitellini, N., Gràcia, E., Matias, L., Terrinha, P., Abreu, M.A., DeAlteriis, G., Henriët, J.P., Dañobeitia, J.J., Masson, D.G., Mulder, T., Ramella, R., Somoza, L., Diez, S., 2009. The quest for the Africa–Eurasia plate boundary west of the Strait of Gibraltar. *Earth Planet. Sci. Lett.* 280, 13–50.